Rowan University

Rowan Digital Works

Neutralizing antibodies against EBV gp42 show potent in vivo protection and define novel epitopes

Qian Wu

Ling Zhong

Dongmei Wei

Wanlin Zhang

Junping Hong

See next page for additional authors

Recommended Citation

Authors

Qian Wu, Ling Zhong, Dongmei Wei, Wanlin Zhang, Junping Hong, Yinfeng Kang, Kaiyun Chen, Yang Huang, Qingbing Zheng, Miao Xu, Mu-Sheng Zeng, Yi-Xin Zeng, Ningshao Xia, Qinjian Zhao, Claude Krummenacher, Yixin Chen, and Xiao Zhang

Neutralizing antibodies against EBV gp42 show potent *in vivo* protection and define novel epitopes
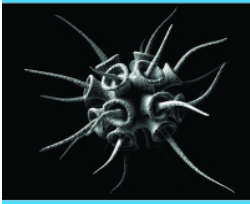
Qian Wu, Ling Zhong, Dongmei Wei, Wanlin Zhang, Junping Hong, Yinfeng Kang, Kaiyun Chen, Yang Huang, Qingbing Zheng, Miao Xu, Mu-Sheng Zeng, Yi-Xin Zeng, Ningshao Xia, Qinjian Zhao, Claude Krummenacher, Yixin Chen & Xiao Zhang

Taylor & Francis
Taylor & Francis Group

Neutralizing antibodies against EBV gp42 show potent *in vivo* protection and define novel epitopes

Qian Wu[a]*, Ling Zhong[b,c]*, Dongmei Wei[a]*, Wanlin Zhang[c]*, Junping Hong[a]*, Yinfeng Kang[c], Kaiyun Chen[a], Yang Huang[a], Qingbing Zheng[a], Miao Xu[c], Mu-Sheng Zeng[c], Yi-Xin Zeng[c], Ningshao Xia [a], Qinjian Zhao[b], Claude Krummenacher[d], Yixin Chen[a] and Xiao Zhang[b]

[a]State Key Laboratory of Vaccines for Infectious Diseases, National Institute of Diagnostics and Vaccine Development in Infectious Diseases, Collaborative Innovation Center of Biologic Products, National Innovation Platform for Industry-Education Integration in Vaccine Research, School of Life Sciences, School of Public Health, Xiang An Biomedicine Laboratory, Xiamen University, Xiamen, People's Republic of China; [b]College of Pharmacy, Chongqing Medical University, Chongqing, People's Republic of China; [c]State Key Laboratory of Oncology in South China, Collaborative Innovation Center for Cancer Medicine, Department of Experimental Research, Sun Yat-sen University Cancer Center, Sun Yat-sen University, Guangzhou, People's Republic of China; [d]Department of Biological and Biomedical Sciences, Rowan University, Glassboro, NJ, USA

ABSTRACT
Epstein–Barr virus (EBV) is the first reported human oncogenic virus and infects more than 95% of the human population worldwide. EBV latent infection in B lymphocytes is essential for viral persistence. Glycoprotein gp42 is an indispensable member of the triggering complex for EBV entry into B cells. The C-type lectin domain (CTLD) of gp42 plays a key role in receptor binding and is the major target of neutralizing antibodies. Here, we isolated two rabbit antibodies, 1A7 and 6G7, targeting gp42 CTLD with potent neutralizing activity against B cell infection. Antibody 6G7 efficiently protects humanized mice from lethal EBV challenge and EBV-induced lymphoma. Neutralizing epitopes targeted by antibodies 1A7 and 6G7 are distinct and novel. Antibody 6G7 blocks gp42 binding to B cell surface and both 1A7 and 6G7 inhibit membrane fusion with B cells. Furthermore, 1A7- and 6G7-like antibodies in immunized sera are major contributors to B cell neutralization. This study demonstrates that anti-gp42 neutralizing antibodies are effective in inhibiting EBV infection and sheds light on the design of gp42-based vaccines and therapeutics.

Introduction

Epstein–Barr virus (EBV) is a ubiquitous member of the γ-herpesvirus subfamily, which establishes lifelong latency in 95% of the human population [1]. EBV predominantly infects epithelial cells and B cells, and persists in latently infected B lymphocytes [2]. EBV infections during childhood and adolescence are usually asymptomatic but may cause infectious mononucleosis (IM) [3]. As an oncogenic virus, EBV is implicated in multiple malignancies including nasopharyngeal carcinoma, gastric cancer and lymphomas such as Hodgkin's lymphoma, natural killer/T cell lymphoma and Burkitt's lymphoma [4]. EBV is associated with approximately 200,000 new cases of malignancies and causes 140,000 deaths each year worldwide. Moreover, EBV infection results in a 32-fold increased risk of developing multiple sclerosis [5,6]. Recently, EBV reactivation was reported to enhance COVID-19 severity [7]. However, effective vaccines and therapeutics against EBV infection remain unavailable so far [8].

EBV entry into cells is a complex process involving multiple viral envelope glycoproteins and various cell receptors [9]. Among the thirteen EBV envelope glycoproteins, BMRF2, gp350, gp42, gB, gH and gL are considered as the essential components for virus attachment, receptor binding and membrane fusion [9]. Both gp350 and gp42 are unique to EBV and are involved in B cell infection [10]. gp350 is the most abundant envelope glycoprotein on the virion surface and is involved in attachment to the target cell surface through binding to complement receptor type 2 (CR2/CD21) or to CR1 (CD35) [11,12]. Because of this, EBV prophylactic vaccines tested in clinical trials have mostly focused on gp350 [8]. However, a candidate vaccine based on a soluble form of gp350 failed to prevent asymptomatic infection in a phase II clinical trial, even though the incidence of IM decreased [13].

Although gp350 promotes infection efficiency, it is not strictly indispensable for virus infection [14]. In contrast, gp42 is an essential glycoprotein involved in EBV infection of B cells. Virions lacking gp42 maintain the ability of attaching to B cells but subsequently fail to enter these cells [15]. Importantly, antibodies against gp42 found in plasma of naturally infected individuals contribute to B cell neutralization [16]. Moreover, a nanoparticle vaccine containing gp42 elicited a potent B cell neutralizing antibody response in mice and nonhuman primates [16]. Therefore, gp42 is becoming a key component in the development of promising EBV vaccine candidates.

EBV mainly infects epithelial cells and B cells, and gp42 serves as a cell tropism switch [17]. gp42 is associated with the gH/gL heterodimer to form the entry complex that activates the fusogen gB during entry into B cells [18]. Interaction between gp42 and human leukocyte antigen class II (HLA-II) molecules is essential for B cell infection, while gp42 binding to gH/gL significantly interferes with virus entry into epithelial cells [19]. Virions secreted from B cells usually carry a lower amount of gp42 since intracellular gp42 binds to HLA-II and is degraded [20]. Hence, virions produced from B cells are highly epithelial cell-tropic. In contrast, virions generated from epithelial cells (HLA-II negative) have a higher content of gp42 on the virus envelope, which directs these virions to infect B cells expressing the HLA-II receptor.

EBV gp42 is a type II transmembrane glycoprotein encoded by the BZLF2 gene [21]. Two forms of gp42 are generated in infected cells: a full-length form with its transmembrane region and a N-terminally truncated soluble form [22]. Both forms are functional in immune evasion by hampering HLA-II-restricted antigen presentation [23]. Additionally, gp42 binding to HLA-II blocks the recognition of HLA-II-peptide complexes by T cell receptors (TCR), which reduces the activation of CD4$^+$ T cell [24,25].

The gp42 ectodomain contains four N-linked glycosylation sites at residues N64, N93, N98 and N173 [23,26,27], and can be divided into a flexible N-terminal domain and a C-terminal domain [28]. The gp42 N-terminal domain wraps around three gH domains with nanomolar affinity, and its deletion reduces fusion efficiency with B cells [22,29]. However, the gp42 N-terminal domain inhibits gH/gL tethering to receptors during epithelial cell infection [30]. Synthetic peptides derived from the gp42 N-terminal domain bind to gH/gL with high affinity and inhibit epithelial cell fusion [31,32]. Thus, the N-terminus of the gp42 ectodomain is the functional regulator of cell tropism for EBV. During entry into B cells, gp42 serves as the bridge between EBV and host cells by interacting with HLA-II and activating the gH/gL complex, which further activates gB to effect membrane fusion [29]. The EBV B cell entry process depends on the interaction between the gH/gL/gp42 complex and HLA-II, mediated by the C-terminus of the gp42 ectodomain [18]. gp42 belongs to the C-type lectin superfamily and contains a C-type lectin domain (CTLD) to engage in HLA-II binding [26,33]. Mutation analyses showed that amino acid substitution, insertion and deletion in the gp42 C-terminal domain significantly impaired binding to HLA-II and B cell fusion [31,34–36]. In summary, gp42 plays a vital role in receptor binding and promoting membrane fusion for infection of B cells, thereby providing a promising target for neutralizing antibody screening and vaccine design.

Considering the complexity of EBV entry into cells and the involvement of multiple viral glycoproteins, it will be an effective vaccine strategy to combine different EBV antigens [8]. However, to rationally assemble a combination of antigens, it is important to identify neutralizing epitopes of individual glycoproteins [37]. Multiple neutralizing antibodies targeting other glycoproteins including gp350, gB and gHgL have been reported [9,38]. Nevertheless, only few antibodies targeting gp42 are known, thus, the present study focuses on characterizing the neutralizing response to gp42.

In the present study, we report two novel rabbit neutralizing antibodies (NAbs), 1A7 and 6G7. Both 1A7 and 6G7 showed comparable neutralizing ability in a B cell infection model, and 6G7 effectively protected humanized mice from lethal EBV challenge. Epitope competition analysis and epitope mapping results revealed that 1A7 and 6G7 recognize distinct regions located in the C-terminal domain of gp42. Only 6G7 was capable of inhibiting the attachment of gp42 to B cell surface. However, both 1A7 and 6G7 were able to prevent membrane fusion with B cells. The epitopes recognized by 1A7 and 6G7 are immunodominant for induction of neutralizing antibodies. These two NAbs and their epitopes provide new insight for the design of gp42-based vaccines against EBV infection.

Materials and methods

Experimental details on plasmid construction, protein expression and purification, enzyme linked immunosorbent assay, cell surface staining of gp42 by flow cytometry, surface staining of gp42 by immunofluorescence, surface plasmon resonance (SPR) assays, SDS-PAGE and western blot, deglycosylation of gp42, virus production, neutralization assay on B cells, cell surface binding assays, virus-free cell fusion assay, immunization with immune complex and statistical analysis are described in the Supplementary document, Materials and Methods.

Human specimens

Sera from healthy individuals and NPC patients were collected from Sun Yat-sen University Cancer Center. This study was approved by the Institutional Ethics Committee of the Sun Yat-sen University Cancer Center, Guangdong, China. Written informed consent was obtained from all participants.

Rabbit B cell isolation and recombinant antibody construction

10-week-old New Zealand White Rabbits (Songlian Laboratory Animal Center, Shanghai) were subcutaneously immunized with 300 μg gp42-His protein mixed with an equal volume of Freund's adjuvant three times at 2-week intervals. 4 weeks after the final immunization, approximately 5 mL of blood was collected. Peripheral blood mononuclear cells (PBMCs) were isolated by Ficoll-Paque PLUS (GE Healthcare) according to the manufacturer's protocol. Briefly, whole blood was diluted with one volume of serum-free RPMI 1640 (Sigma-Aldrich), and the mixture was layered onto Ficoll-Paque PLUS before centrifugation at 800 g for 30 min at room temperature. The PBMC layer was collected and washed three times with PBS.

To sort antigen-specific B cells, Sulfo-NHS-LC-Biotin (Thermo Fisher Scientific) conjugated gp42-His was used. PBMCs were suspended in 100 μL PBS and incubated with biotin conjugated gp42-His for 30 min at 4 °C. The mixture was then washed three times with PBS and pelleted by centrifugation at 800 g for 5 min. PBMCs were then incubated with Streptavidin APC Conjugate (Thermo Fisher) and labelled for a panel of markers by incubation with LIVE/DEAD Aqua (Thermo Fisher), Mouse anti Rabbit CD4: FITC (Biorad), Mouse anti Rabbit CD8: FITC (Biorad), Mouse anti Rabbit T Lymphocytes: FITC (Biorad), Mouse anti Rabbit IgM: RPE (Biorad). B cell sorting was carried out on a BD FACS Aria III cell sorter as previously described [39].

The RNA of single gp42-positive B cells was extracted and followed by cDNA preparation using Superscript III reverse transcriptase (Invitrogen) primed with random hexamer. Antibody variable region genes were recovered via two rounds of PCR using GXL polymerase (Takara) and then inserted into pVRC8400 vectors containing the constant region of rabbit heavy chain or light chain. The plasmids pVRC8400-1A7-L encoding the light chain and pVRC8400-1A7-H encoding the heavy chain were used to express 1A7. The plasmids pVRC8400-6G7-L encoding the light chain and pVRC8400-6G7-H encoding the heavy chain were used to express 6G7.

EBV challenge in humanized mice

All animal experiments were performed under protocols approved by the Sun Yat-sen University Cancer Center Animal Care and Use Committee. According to approved guidelines, animals were humanely euthanized at the end of experiments.

The humanized mice were established by engrafting CD34$^+$ human hematopoietic stem cells obtained from umbilical cord blood into NOD.Cg-Prkdce-m1IDMOIl2rgem2IDMO (NOD-Prkdcnull IL2Rγ-null, NPI®) mice (BEIJING IDMO Co., Ltd). Antibodies of experimental or control group were intraperitoneally (i.p.) injected with a dose of 400 μg (20 mg/kg). After 24 h, the mice received a dose of Akata-EBV-GFP (25,000 green Raji unit (GRU)) via intravenous (i.v.) route. In the following four weeks, the mice received the same dose of antibodies (400 μg/mouse) weekly. Blood samples were collected and body weights were recorded weekly. The mice were euthanized 7 weeks post challenge or earlier if they have more than 20% of the body weight loss.

Viral DNA was extracted from peripheral blood, sera or spleens of humanized mice using DNA extraction kits (Omega) according to the manufacturer's instructions. EBV DNA copy numbers were measured by real-time polymerase chain reaction (QuantiFast SYBR Green RT–PCR Kit; Qiagen) using primers specific for BALF5 (F: 5'-GGTCACAATCTC-CACGCTGA-3'; R: 5'-CAACGAGGCTGACCT-GATCC-3'). The DNA copy numbers were quantified using a standard curve plotted with a serially diluted plasmid of pUC19-BALF5.

Anti-EBV VCA IgG, anti-EBV VCA IgM and anti-EBV EBNA1 titres of sera collected from humanized mice were detected by commercial VCA-IgG kit (Euroimmun), VCA-IgM kit (Euroimmun) and EBNA1-IgG kit (Euroimmun) according to the manufacturers' instructions.

At the time of euthanasia, mouse spleens were fixed in 10% formalin and embedded in paraffin. Spleen sections from different groups were stained with hematoxylin and eosin (H&E). We used a commercial kit (ZSGB-BIO) to detect the Epstein–Barr virus-encoded RNAs (EBERs) by in situ hybridization (ISH). Human B cells were stained by immunohistochemistry (IHC) using hCD20 antibody (Abcam) at 1:200 dilution.

For the immunophenotype analysis of PBMCs and splenocytes, cells were stained with antibodies including anti-human CD45-APC/Cy7, CD19-APC, CD3-FITC, CD4-pacific blue, CD8-PC5.5 and anti-mouse CD45-BV510 (Biolegend) for 30 min at 4°C. Detection of human plasmablastic immunophenotype B cells was performed by staining with anti-human CD45-APC/Cy7, CD19-APC, CD38-BV650, CD24-PC5.5 and anti-mouse CD45-BV510 (Biolegend). Detection of human activated T cells was performed

by staining with anti-human CD45-APC/Cy7, CD3-FITC, CD8-PC5.5, CD69-PC7, CD137-APC and anti-mouse CD45-BV510 (Biolegend). For the intracellular molecule staining, splenocytes were seeded in 96-well round bottom plates and stimulated with 10 µg EBV EBNA1 protein for 12 h with 2 µM monensin (BioLegend) and 5 µg/mL brefeldin A (BioLegend) added at the 8 h. Splenocytes stimulated with SARS-CoV-2 S protein and stimulated with phorbol myristate acetate (PMA)-ionomycin (Sigma) stimulation, were used as a negative control and a positive control, respectively. After stimulation, cells were collected, washed and stained with anti-human CD45-APC/Cy7, CD3-FITC, CD4-pacific blue and CD8-PC5.5 (BioLegend). After fixed and permeabilized with 1×Fixation Buffer/Permeabilization Wash Buffer (BioLegend), cells were stained with TNF-α-BV650 (BioLegend). Data were collected with CytoFLEX (Beckman Coulter) and analysed using FlowJo software X 10.0.7 (Tree Star).

Results

Characterization of anti-EBV gp42 rabbit monoclonal antibodies

The ectodomain of gp42 (amino acids 36–223) was expressed in 293F cells and used for rabbit immunization. We isolated gp42-specific memory B-cells from peripheral blood mononuclear cells (PBMCs) of immunized rabbits. The variable regions encoding the heavy and light chains were amplified from separate single B cells and cloned into a pVRC8400 vector containing rabbit IgG constant regions to produce antibodies as previously described [39]. We successfully obtained two gp42-specific antibodies, named 1A7 and 6G7. Specific binding activities against gp42 was tested by indirect enzyme linked immunosorbent assay (ELISA) and showed a mean half-maximal effective concentration (EC_{50}) of 27.15 ng/mL for 1A7 and 17.89 ng/mL for 6G7 (Figure 1(A)). The control antibody, 9E1 (anti-SARS-Cov-2 mAb) [39], did not react with gp42. The equilibrium dissociation constant (KD) measured by surface plasmon resonance (SPR) demonstrated that both antibodies bind with nanomolar affinities (Figure 1(B)). In particular, 6G7 showed about a 5-fold higher binding affinity (1.13 nM) for gp42 than 1A7 (5.78 nM) (Figure 1(B)). Next, we investigated whether 1A7 and 6G7 could bind to full-length gp42 anchored on the cell surface. 293T and 293β5 cells were transfected with a plasmid expressing full-length gp42. Results from flow cytometry and immunofluorescence (IF) assays indicated that both 1A7 and 6G7 recognized gp42 on the cell surface to a similar extent (Figure 1(C,D)). To start determining whether 1A7 and 6G7 recognize overlapping epitopes, we tested whether 1A7 and 6G7 could bind to gp42 simultaneously by SPR (Figure 1(E,F)). The increase in signal when both antibodies are present, over each individual antibody, suggests that the epitopes recognized by these two antibodies are distinct. We further evaluated 1A7 and 6G7 neutralizing ability using a B cell infection model. In this assay 6G7 showed a potent neutralizing ability with the half maximal inhibitory concentration (IC_{50}) value of 0.28 µg/mL. This value is slightly better than the IC_{50} value (0.41 µg/mL) of the well-characterized anti-gp350 neutralizing antibody 72A1 [40] (Figure 1(G)). In contrast, 1A7 had a higher IC_{50} concentration and could only achieve 65% neutralization overall. The results demonstrated that the two new anti-gp42 antibodies 1A7 and 6G7 efficiently recognized both recombinant and native forms of gp42. Data also showed that these antibodies recognized different epitopes, bound with slightly different affinity and were able to prevent EBV infection of B cells *in vitro*.

Antibody 6G7 conferred protection against lethal challenge in humanized mice

Several anti-gp42 antibodies have been reported to neutralize EBV infection of B cells *in vitro* [41,42]. Since antibody 6G7 showed better neutralizing efficacy than 1A7 in B cell infection (Figure 1(G)), we used a humanized mouse model to further examine the protective potential of 6G7 *in vivo*. The humanized mice were established by engrafting cord blood-derived $CD34^+$ human hematopoietic stem cells into the NOD-$Prkdc^{null}$ $IL2R\gamma^{null}$ (NPI) mice [43]. To reduce the antibody's immunogenicity in humanized mice, the rabbit IgG constant regions of 6G7 were replaced with human IgG1 constant regions as described previously [44]. The recently reported anti-gH/gL antibody, AMMO1 [45], was chosen as the positive control and an anti-HIV NAb, VRC01 [46], was used as the negative control. The experimental procedure was shown in Figure 2 (A). Briefly, 400 µg (20 mg/kg) of chimeric 6G7, AMMO1 or VRC01 were administered to humanized mice via intraperitoneal (i.p.) route. 24 h later, mice received an intravenous (i.v.) injection of Akata-EBV equivalent to ~25,000 green Raji units (GRU) per mouse. In the following 4 weeks, the same dose of antibodies was delivered weekly. The animals were bled weekly and monitored for body weight change, survival rate, EBV DNA copy numbers and immune cell dynamic change. Mice were euthanized at week 7 or earlier when the mice were clinically ill, and tissue pathology was evaluated.

Peripheral blood was collected weekly and viral DNA load was measured by RT–PCR (Figure 2(B)). The EBV DNA copy numbers of mice treated with VRC01 became detectable and increased rapidly from week 2 (Figure 2(B)). Furthermore, EBV DNA copy number in the remaining VRC01-treated mouse
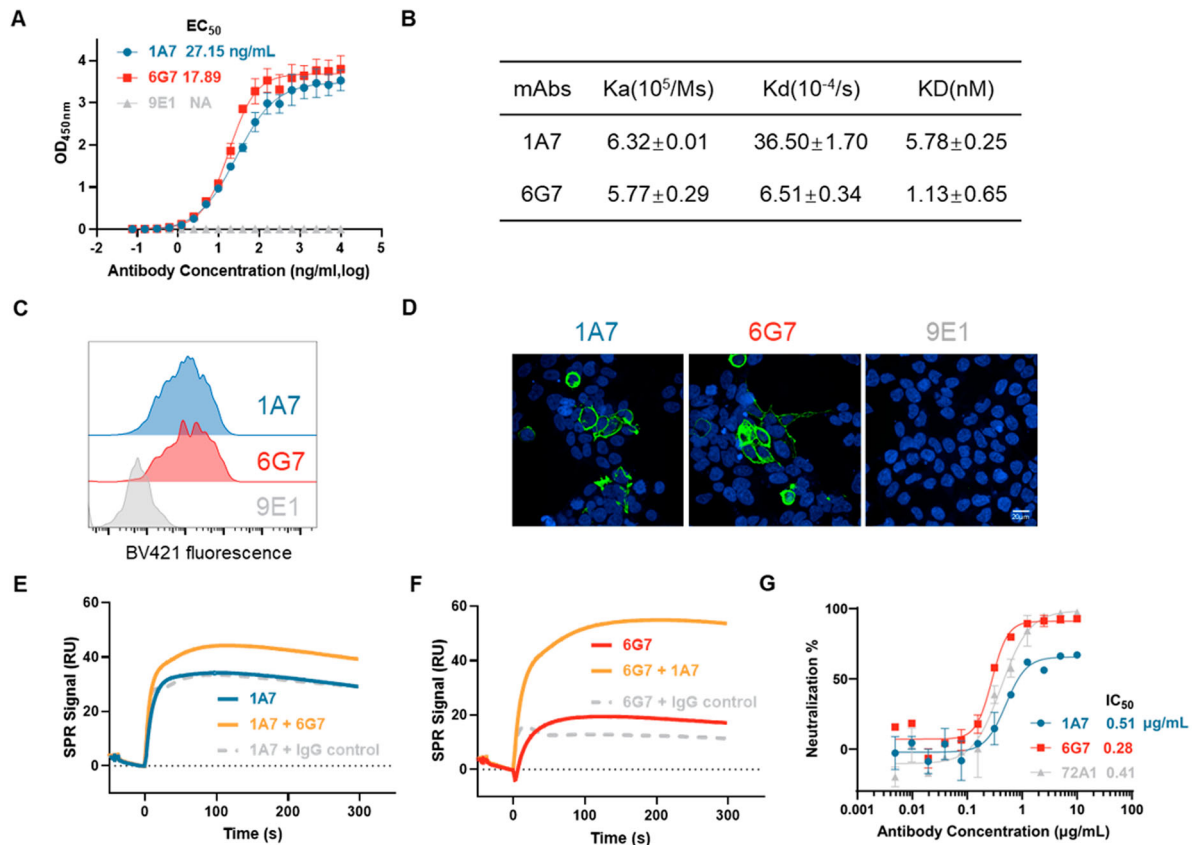
Figure 1. Characterization of anti-EBV-gp42 rabbit mAbs. (A) Binding of 1A7 and 6G7 antibodies to EBV gp42 ectodomain was tested by ELISA. The half maximal effective concentration (EC_{50}) values were calculated by four parameters nonlinear regression. Antibody 9E1 (SARS-Cov-2) acts as a negative control. Error bars represent SEM of three experiments. (B) The binding affinity of antibodies to gp42 was measured by SPR. The values of the rate of association (Ka), rate of dissociation (Kd) and affinity constant (KD) are shown as the mean ± SD of three experiments. (C) Antibody binding to cell surface-expressed gp42 in transfected 293T cells was evaluated by flow cytometry. (D) Antibody binding to cell surface-expressed gp42 in transfected 293β5 cells was evaluated by immunofluorescence. Bound antibodies were detected with secondary anti-rabbit-AlexaFluor488 antibody (green), cell nuclei were stained with DAPI (blue). (E) and (F) The simultaneous binding of 1A7 and 6G7 antibodies was examined by SPR. Binding signal of each antibody alone was compared to the binding signal when a combination of both antibodies was used. The 300-second association phase is shown for representative experiments. (G) The neutralizing activity of antibodies was evaluated in a B cell infection assay. Curves were fit by four parameters nonlinear regression and half-maximal inhibitory concentration (IC_{50}) was calculated.

exceeded 10^5 copies/μL at week 7 (Figure 2(B)). The increase of DNA copies in the blood of control mice reflects serious viremia. Mice that received 6G7 and AMMO1 antibodies had a low amount of viral DNA peripheral blood, which steadily remained under the detectable amount (10 copies/μL) through the entire experiment (Figure 2(B)). EBV infection led to physiological loss of body weight of mice treated with VRC01. The body weight of VRC01-treated mice continued to decline from week 2 and dropped to 75% at week 7 (Figure 2(C)). Five of six mice from the VRC01-treated group naturally died or were euthanized (body weight loss more than 20%), while AMMO1 and 6G7-treated mice all survived during the experiment (Figure 2 (D)). In contrast, all the mice that received 6G7 or AMMO1 antibodies survived and maintained a relatively steady body weight (Figure 2(C,D)).

We further analysed the lymphocytes in peripheral blood of humanized mice (Table S1). All humanized mice had similar ratio of human CD45+ (hCD45+)

cells in the total CD45+ cells (Figure 2(E)). However, mice from the VRC01-treated group showed a significant decline in the frequency of peripheral hCD19+ B cells, concurrent with a marked increase of hCD3+ T cells (Figure 2(F,G)). The increase of hCD3+ T cells was mainly due to the increase of hCD8+ cytotoxic T lymphocytes (CTL) but not hCD4+ T cells (Figure 2 (H,I)). hCD8+ CTL may eliminate EBV-infected hCD19+ B cells leading to the decreasing of B cells (Figure 2(F,I)) [47]. Mice that received 6G7 and AMMO1 retained a steady level of peripheral hCD19+ B cells and hCD3+ T cells (Figure 2(F,G)). In summary, 6G7 or AMMO1 treatment controlled EBV infection and EBV viremia after lethal EBV challenge *in vivo*.

Antibody 6G7 protected humanized mice from EBV-induced lymphoma

We further evaluated the pathological changes of spleens of infected humanized mice treated with
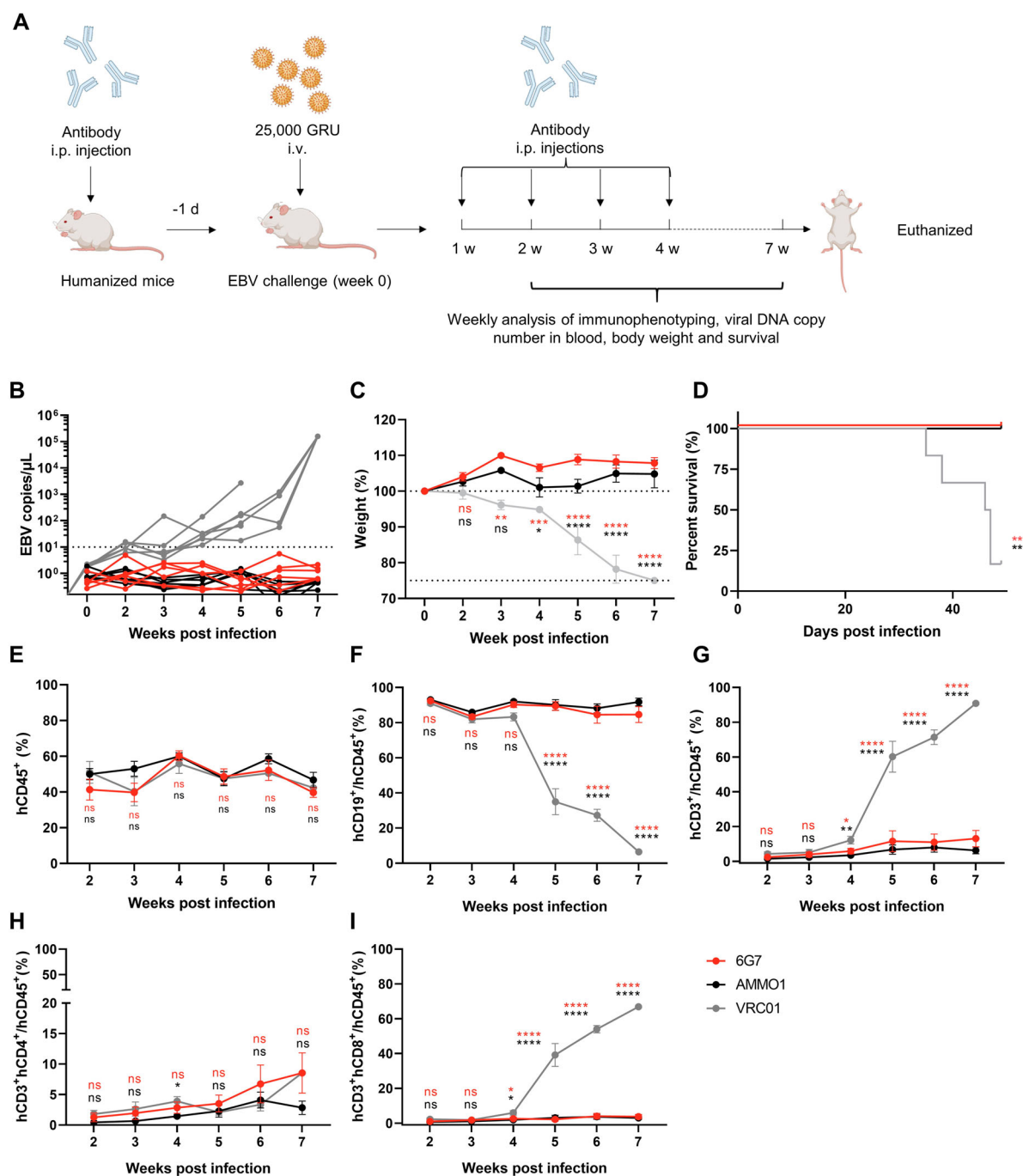
Figure 2. Protection efficiency of 6G7 antibody in a humanized mouse model. (A) Experimental timeline for antibodies delivery, virus challenge, and monitoring for biological and clinical outcomes of humanized mice ($n = 6$ for each group). Mice were euthanized at week 7. i.p.: intraperitoneal, i.v.: intravenous. (B) Viral DNA copy numbers in peripheral blood over time were determined by quantitative RT-PCR. The dashed line indicates the detection limit. Each line represents an individual mouse. (C) Body weight measured over time. Each line represents the average weight of the indicated group as percent change of original weight. (D) Percentage of survival over time. The frequency and change of (E) hCD45$^+$, (F) hCD19$^+$, (G) hCD3$^+$, (H) hCD4$^+$ and (I) hCD8$^+$ in the peripheral blood of humanized mice were monitored over the experiment period. Statistical analyses were performed using one-way ANOVA. The colour of the asterisks denotes the group with which there is a significant difference from the VRC01 control group determined by a Sidak multiple comparison test. All data are presented as mean ± SEM. **$P \leq 0.0021$; ****$P \leq 0.0001$. ns: no significant difference. Schematic diagram was made with BioRender.com.

different antibodies. The spleens from VRC01-treated mice were visibly enlarged and heavier (Figure 3(A, B)). Irregular and pale tumours were also observed on the surface of spleens of VRC01-treated mice, while spleens from 6G7 and AMMO1-treated mice showed normal size and weight without tumour

formation (Figure 3(A,B)). We further analysed spleen sections using hematoxylin and eosin (H&E) staining, immunohistochemistry (IHC) for hCD20, as well as *in situ* hybridization for Epstein–Barr virus-encoded RNA (EBER). Tumour regions in enlarged spleens from VRC01-treated mice showed abundant positive
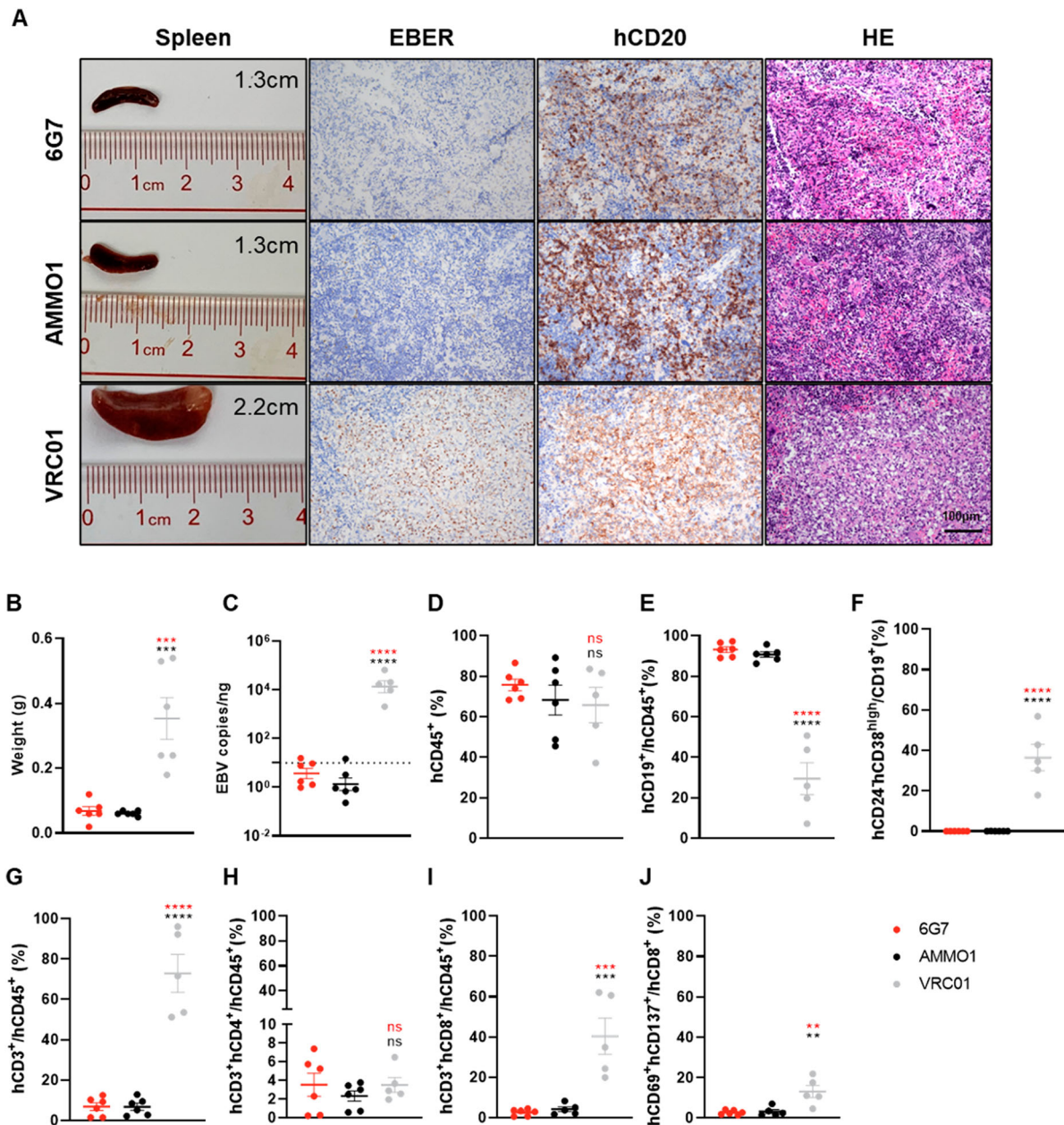
Figure 3. 6G7 reduced EBV replication in spleen and prevented EBV-induced lymphoma. (A) Representative macroscopic images of spleens from infected humanized mice from the three groups are shown. Corresponding splenic sections stained for EBV encoded RNA (EBER), human CD20 (hCD20) and hematoxylin and eosin (H&E) are shown for each group. The scale bar (100 μm) for microscopy images is indicated. (B) The weight of spleens of individual mice at time of euthanasia is shown. (C) EBV DNA copy numbers per ng of DNA from spleen were determined by RT-PCR. (D-J) The frequency of (D) hCD45$^+$, (E) hCD19$^+$, (F) hCD24$^-$hCD38^{high}, (G) hCD3$^+$, (H) hCD4$^+$, (I) hCD8$^+$ and (J) hCD69$^+$hCD137$^+$ cells in spleens were evaluated. For each analysis of C–F, $n = 6$ for 6G7 and AMMO1-treated group and $n = 5$ for the VRC01 group since one mouse died naturally on day 46. Statistical analyses were performed using one-way ANOVA. The colour of the asterisks denotes groups that were significantly different from the negative control group (VRC01 treated) using a Sidak multiple comparisons test. All data are presented as mean ± SEM. **$P \leq 0.0021$; ***$P \leq 0.0002$; ****$P \leq 0.0001$; ns, no significant difference.

staining for EBER and hCD20 (Figure 3(A)), which resulted from proliferation of EBV-infected human B cells. These observations are consistent with typical symptom of large B-cell lymphomas in this model [47]. Consistent with the result of EBER staining, mice from the VRC01-treated group showed 1000-fold higher levels of EBV DNA than those treated with 6G7 or AMMO1 (Figure 3(A,C)).

Moreover, analysis of human lymphocytes in these spleens showed that similar proportions of hCD45$^+$

cells were observed in spleens of mice from the different groups (Figure 3(D), Table S1). A significant decrease in hCD19$^+$ B cells was detected in the spleens from VRC01-treated mice when compared to 6G7 and AMMO1-treated mice (Figure 3(E)). However, the frequency of plasmablastic B cells (hCD19$^+$ hCD24$^-$hCD38^{high}) increased dramatically in the VRC01 group (Figure 3(F)). This observation is consistent with lymphocyte changes in peripheral blood of VRC01-treated mice (Figure 2(F–I)). The

proportion of hCD3^{+} and hCD8^{+} T cells increased and hCD4^{+} T cells remained stable, concomitantly with a decrease in the frequency of hCD19^{+} B cells (Figure 3(E,G–I)). Besides, the percentage of activated hCD8^{+} T cells (hCD69^{+}/hCD137^{+}) in the VRC01-treated group was significantly higher than in spleens of 6G7 and AMMO1-treated mice (Figure 3(J)).

In humanized mice, which lack their native immune system, the engrafted human cells do not reconstitute a full humoral immune response. In particular, the development of "human" germinal centres and secondary lymphoid tissues is not sufficient for the analysis of a human humoral immune response [48,49]. Therefore, antibody production cannot generally be evaluated in the current humanized mice models. Hence, the VCA-IgG, VCA-IgM and EBNA1-IgG antibody titres used to define the infection status in human is not suitable for this model [50]. As expected, no anti-VCA IgG, anti-VCA IgM and anti-EBNA1 IgG antibodies were detected in mice treated by 6G7 or AMMO1, or with the negative control mAb VRC01 (Fig. S1A-S1C). The EBV viral load in sera of mice treated by VRC01 significantly increased 2 weeks post viral challenge (Fig. S1D). In contrast, EBV DNA remained undetectable in sera from mice treated by 6G7 or AMMO1, which is consistent with EBV viral loads in whole blood (Figure 2 (B) and Fig. S1D). These data confirmed that EBV lytic infection occurred only in mice from the control group where new virus may be released into serum. Furthermore, we assessed T cell responses to EBV EBNA1 by restimulating splenocytes of mice treated by different antibodies with EBNA1 protein or with a control protein, SARS-CoV-2 S for 12 h *in vitro*. EBNA1-specific T cells were detected in control mice treated by VRC01, indicating that infection in the VRC01-group induced a T cell response (Fig. S1E and S1F) [47]. In contrast, no EBNA1-specific T cells were detected in 6G7- and AMMO1-treated mice indicating that these antibodies completely neutralized viral infection (Fig. S1E and S1F).

Overall, these data demonstrated that anti-gp42 6G7 and AMMO1 antibodies completely protected humanized mice from EBV infection and prevented formation of EBV-induced lymphoma by inhibiting viral infection of B cells in the humanized mouse model.

Epitope mapping of 1A7 and 6G7 antibodies

In order to identify the epitopes recognized by the 1A7 and 6G7 antibodies, we first tested their cross-reactivity with rhesus lymphocryptovirus (rhLCV) gp42. rhLCV is an EBV homolog of non-human primates, which is frequently used as a surrogate for EBV-related studies. Despite a 77.6% similarity of amino acid sequences between EBV and rhLCV gp42 (Fig.

S2) [51], antibodies 1A7 and 6G7 did not cross-react with rhLCV gp42 (Fig. S3), indicating that the epitopes recognized by the two NAbs were specific to EBV gp42. Given the high conservation of glycoprotein structures among herpesvirus, we made a panel of seven chimeric constructs (CC) by replacing continuous regions of rhLCV gp42 with corresponding regions of EBV gp42 (Figure 4(A) and Table S2). Binding of 1A7 and 6G7 to chimeric gp42 constructs was quantified by flow cytometry. We found that binding of 1A7 was only retained in CC-5, which contained only EBV gp42 residues 134–173. In contrast, the 6G7 antibody only detected CC-6, which comprises only EBV gp42 residues 159–198 (Figure 4(B) and Fig. S3). The mapping of the non-overlapping 1A7 and 6G7 epitopes is consistent with the ability of these antibodies to bind simultaneously to EBV gp42 (Figure 1(E)). To further define the epitopes recognized by 1A7 and 6G7, we constructed a series of chimeric constructs based on CC-5 and CC-6 that contain more limited regions of EBV gp42 (Table S2). Three of the four CC-5-derived constructs retained reactivity to 1A7 (Figure 4(C) and Fig. S4A), suggesting that the 1A7 epitope mapped to EBV gp42 residues 149–163 (Table S2). All the new chimeric constructs based on CC-6 were recognized by 6G7 (Figure 4(D) and Fig. S4B), thus narrowing down the 6G7 epitope to EBV gp42 residues 174–183 (Table S2). Even though continuous regions of EBV gp42 were sufficient to allow detection of full-length rhLCV-based chimera expressed at the surface of transfected cells by 1A7 or 6G7, neither antibody could react with denatured gp42 by western blot (Fig. S5). These data indicate that the sequences identified using chimeras belong to conformation-dependent epitopes recognized by 1A7 or 6G7. The sequences recognized by 1A7 and 6G7 were structurally close to each other but oriented in different directions (Figure 4(E,F)). The linear portion of the 1A7 epitope consists of the α2 helix and an adjacent loop region (Figure 4(G)). On the other side of gp42, the linear portion of the 6G7 epitope consists of a loop region from W174 to K183 (Figure 4(H)). Altogether, these epitopes define new sites of EBV gp42 recognized by robustly neutralizing antibodies.

Identification of key residues necessary for binding of 1A7 and 6G7 antibodies

In order to determine the key residues of EBV gp42 necessary for the binding of 1A7 and 6G7 antibodies, we constructed a series of mutants with single alanine substitutions spanning the 1A7 epitope (aa 149–163) and the 6G7 epitope (aa 174–183). Binding of 1A7 and 6G7 to these mutants was evaluated by ELISA. Nine of fourteen single alanine mutations between aa 149 and 163 affected 1A7 binding (Figure 4(I,K)),
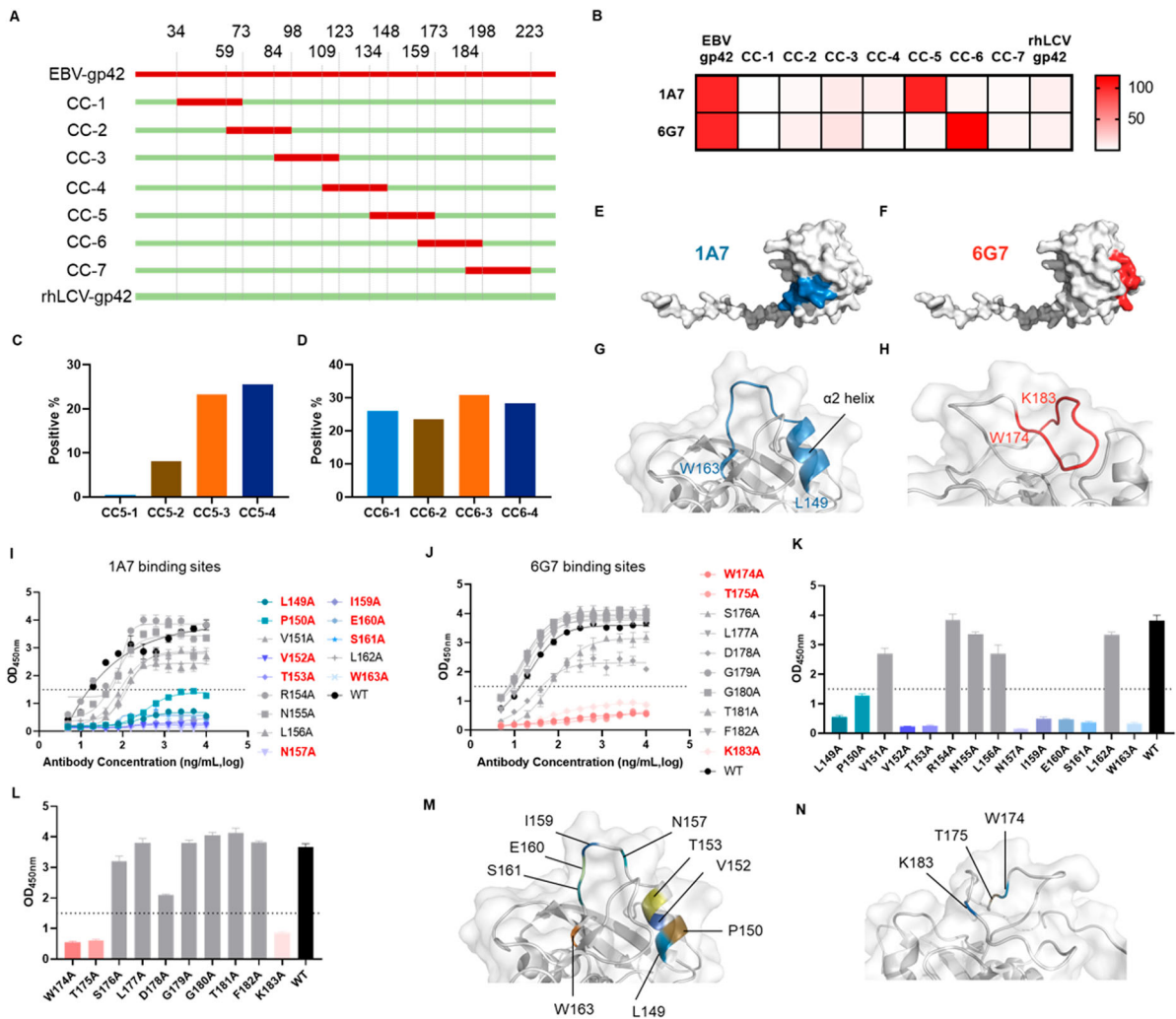
Figure 4. Validation of epitopes defined by 1A7 and 6G7. (A) Schematic representation of chimeric constructs of gp42. rhLCV gp42 (green) was used as the scaffold and different fragments of rhLCV gp42 were replaced by corresponding fragments of EBV gp42 (red). Amino acid numbers correspond to EBV gp42 sequence. (B) Heatmap representing reactivity of 1A7 and 6G7 antibodies against different chimeric constructs (CC-1 to CC-7) determined by flow cytometry. Colour intensities are based on percent reactivity to EBV gp42 (100%). (C) Reactivity of the 1A7 antibody against proteins derived from chimeric construct-5 with shorter EBV-gp42 regions (CC5-1 to CC5-4). The histogram represents the percentage of positive cells determined by flow cytometry (D) Reactivity of the 6G7 antibody against proteins derived from chimeric construct-6 with shorter EBV-gp42 regions (CC6-1 to CC6-4). (E and F) Epitopes of 1A7 and 6G7 are illustrated on the surface of gp42. (G and H) Epitopes of 1A7 and 6G7 are illustrated on a ribbon representation of gp42. (I and J) Binding of serially diluted 1A7 and 6G7 to wild type gp42 (WT) or gp42 mutants were assessed by ELISA. Data represent the average of four experiments ± SEM. (K and L) Binding of 1A7 and 6G7 at a 10µg/mL concentration against wild type gp42 (WT) or gp42 mutants by ELISA is summarized in bar graphs. Colours are consistent with panels I and J. (M and N) The key residues recognized by 1A7 and 6G7 are illustrated. Images were edited using PyMOL from wild type EBV gp42 (PDB: 5T1D).

indicating that most residues in the epitope were necessary for 1A7 interaction. Eight mutations (L149A, V152A, T153A, N157A, I159A, E160A, S161A and W163A) almost completely abolished the interaction between 1A7 and gp42, while some residual binding could be observed for the P150A mutant (Figure 4(I,K)). Four residues (L149, P150, V152 and T153) are located on the α2 helix of gp42 and the others (I159, E160, S161 and W163) are located on the loop near this helix (Figure 5(M)). Among all ten residues of the linear epitope recognized by 6G7, most of the mutants retained their ability to bind the antibody, while three mutations (W174A, T175A and K183A) almost completely

prevented binding (Figure 4(J,L)). Key residues recognized by 6G7 are closely located on the 3D structure of gp42 (Figure 4(N)). In summary, we identified the key residues involved in the recognition of gp42 by neutralizing antibodies 1A7 and 6G7.

The binding ability of antibodies 1A7 and 6G7 was not glycosylation-dependent

The glycosylation of viral glycoproteins is often essential for receptor interaction and/or immune evasion [52]. The extracellular portion of gp42 contains four N-linked glycosylation sites at residues N64, N93, N98 and N173. Of interest, the glycosylation site of
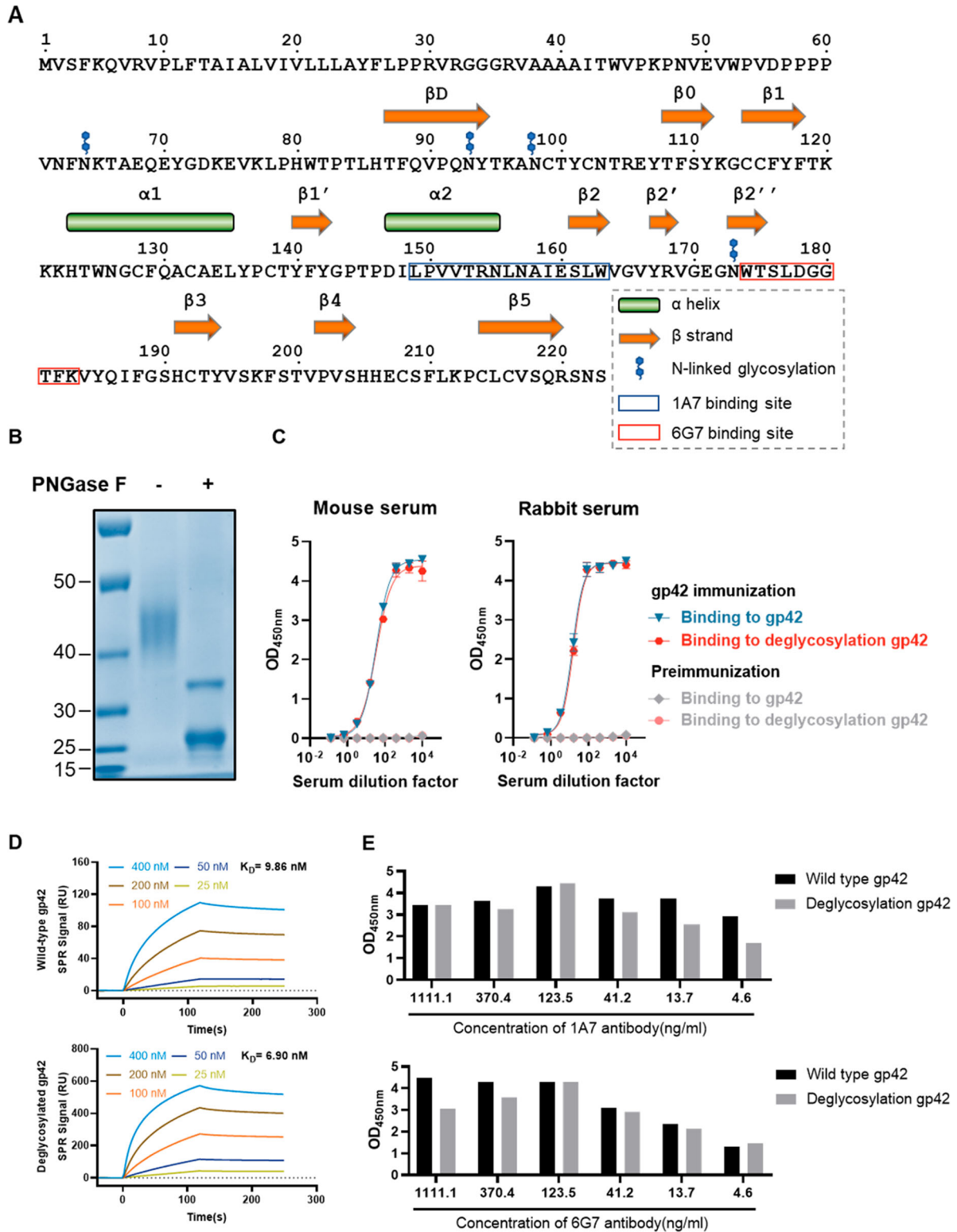
Figure 5. The binding of 1A7 and 6G7 is not influenced by gp42 deglycosylation. (A) Linear graphical representation of EBV gp42 sequence and relevant structural features. Green coils = alpha helices; orange arrows = beta strands; blue hexagon = N-linked glycosylation sites. The 1A7 and 6G7 binding sites are labelled with blue and red box, respectively. (B) SDS-PAGE of wild-type and PNGase F-treated gp42-His stained by Coomassie. The marker indicates protein sizes in kDa. (C) Reactivity of gp42-immunized sera and control sera against wild-type gp42 and deglycosylated gp42 by ELISA. Preimmune sera from mice and rabbits were used as negative controls. (D) The binding affinity of wild type gp42 and deglycosylated gp42- for gH/gL was determined by SPR. Dissociation constant values (KD) were determined using the 1:1 binding model (Biacore 8K). (E) The binding abilities of 1A7 and 6G7 against different forms of gp42 were evaluated by ELISA.

residue N173 is adjacent to the epitope recognized by 6G7 and may partially shield the region (Figure 5(A)). Considering that 1A7 and 6G7 antibodies recognized conformation-dependent epitopes and since glycosylation contribute to conformational stability, we assessed the influence of gp42 deglycosylation on

binding of the two antibodies. PNGase F was used to remove N-linked glycans from gp42-His. After SDS-PAGE, wild-type gp42 appears as a protein smear of 40–45 kDa in size, suggesting heterogeneous glycosylation. After PNGase F treatment, deglycosylated gp42 appears as a band of ~27 kDa in size (Figure 5(B)), consistent with a previous report of deglycosylated gp42 [23]. These data indicate that gp42 is heterogeneously glycosylated at the four potential attachment sites [26]. We first compared the detection of wild type gp42 and deglycosylated gp42 by polyclonal sera from wild type gp42-immunized rabbits and mice. Deglycosylated gp42 and wild type gp42 showed equivalent reactivity with rabbit and mouse polyclonal sera (Figure 5(C)). These ELISA data indicate that deglycosylation had little effect on the overall conformation of gp42 and showed that deglycosylated gp42 retained its overall native antigenicity. One of the essential functions of gp42 is to form an interaction with gH/gL, which is indispensable for infection of B cells. One N-linked glycosylation site (residue N64) is located within the N-terminal domain of gp42, which is tethered to gH/gL. However, residue N64 locates in a linker region (aa 62–66) that is not directly involved in gH/gL binding [29]. As expected, deglycosylation did not affect gp42 binding affinity for gH/gL (Figure 5(D)). Then we investigated the effects of deglycosylation on detection by antibodies 1A7 and 6G7. Both antibodies retained their ability to bind to deglycosylated gp42, indicating that their epitopes were not glycosylation-dependent (Figure 5(E)).

Antibodies 1A7 and 6G7 did not interfere with the formation of the gH/gL/gp42 complex

The formation of the gH/gL/gp42 complex is essential for B cell infection by EBV [18]. To address the mechanism of action of the neutralizing antibodies 1A7 and 6G7, we tested whether they affected formation of the gH/gL/gp42 complex. In particular, the 1A7 epitope mapped closely to gH/gL binding site and shared a common residue (I159) with the gH/gL footprint on the gp42 surface (Figure 6(A)). This proximity suggests that steric hindrance by 1A7 may affect the interaction between gH/gL and gp42. In order to test the influence of antibodies on the interaction between gH/gL and gp42, we performed SPR competition assays. In this test, immobilized gp42 was saturated with either 1A7 or 6G7 immunoglobulin for 400 s, before the addition of soluble gH/gL. After 240 s of association, the RU signal of bound gH/gL was compared between gp42 alone and gp42 saturated with either antibody. Pre-incubation of gp42 with 1A7 or 6G7 did not decrease the amount of gH/gL able to bind to gp42 (Figure 6(B)). We used the same assay to determine whether 1A7 and 6G7 could lead to a decrease of binding affinity between gH/gL and

gp42. The SPR results showed that 1A7 and 6G7 did not impair the affinity of gH/gL for gp42 (Figure 6(C)). Overall, these data indicate that the 1A7 and 6G7 antibodies, despite their high affinity for gp42, had no detectable inhibitory effect on the interaction between gp42 and gH/gL.

The 6G7 antibody inhibited membrane fusion with B cells

During infection of B cells, gp42, especially its C-terminal domain, plays an essential role through binding to the receptor HLA-II [33]. We located the epitopes of 1A7 and 6G7 antibodies on the gp42 C-terminal domain (Figure 4(E,F)). Thus, we used flow cytometry to assess whether these antibodies could affect the binding of gp42, indirectly labelled with PE, to B cells. In this assay, 1A7 only slightly reduced gp42 binding to B cells (Figure 6(D)), even though its epitope partially overlapped with the HLA-II binding site (Fig. S6). In contrast, pre-incubation with 6G7 reduced gp42 binding to B cells (Figure 6(D)), even though the portion of its epitope located on a different side of gp42 without directly overlapping with the HLA-II binding site. We further examined whether these two antibodies could inhibit membrane fusion in a virus-free cell fusion model to reproduce the HLA-II-dependent membrane fusion that occurs during B cell infection. We observed that the efficiency of fusion between glycoprotein-transfected and HLA-II-expressed cells was significantly reduced in the presence of 1A7 or 6G7 antibodies (Figure 6(E)). In contrast the anti-gp350 control antibody, 72A1, had no such effect. To further determine if the 1A7 and 6G7 epitopes were involved in the process leading to membrane fusion, we tested the gp42 mutated at the key residues recognized by 1A7 and 6G7 in this B cell fusion assay. Total and surface expression levels of these mutants compared to wild type gp42 were determined by FCM (Figure 6(F,G,I,J)). The total expression levels of most mutants were impacted except for T153A, S161A, W174A and T175A (Figure 6(F,I)). As for surface expression levels, all mutants were less expressed at the cell surface compared to wild type gp42 (Figure 6(G,J)), which may contribute to reduction in their fusion activity (Figure 6(H,K)). The analysis of key residues recognized by 1A7 showed that mutants L149A, P150A, V152A, I159A and S161A have higher levels of cell surface expression than W163A, while the fusion activity of those mutants was relatively lower or close to W163A (Figure 6(G,H)). Hence, these residues (L149A, P50A, V152A, I159A and S161A) may play an essential role in membrane fusion. A similar analysis of the 6G7 epitope showed that mutant T175A, which displayed a higher expression level and lower fusion activity, may be important for membrane fusion
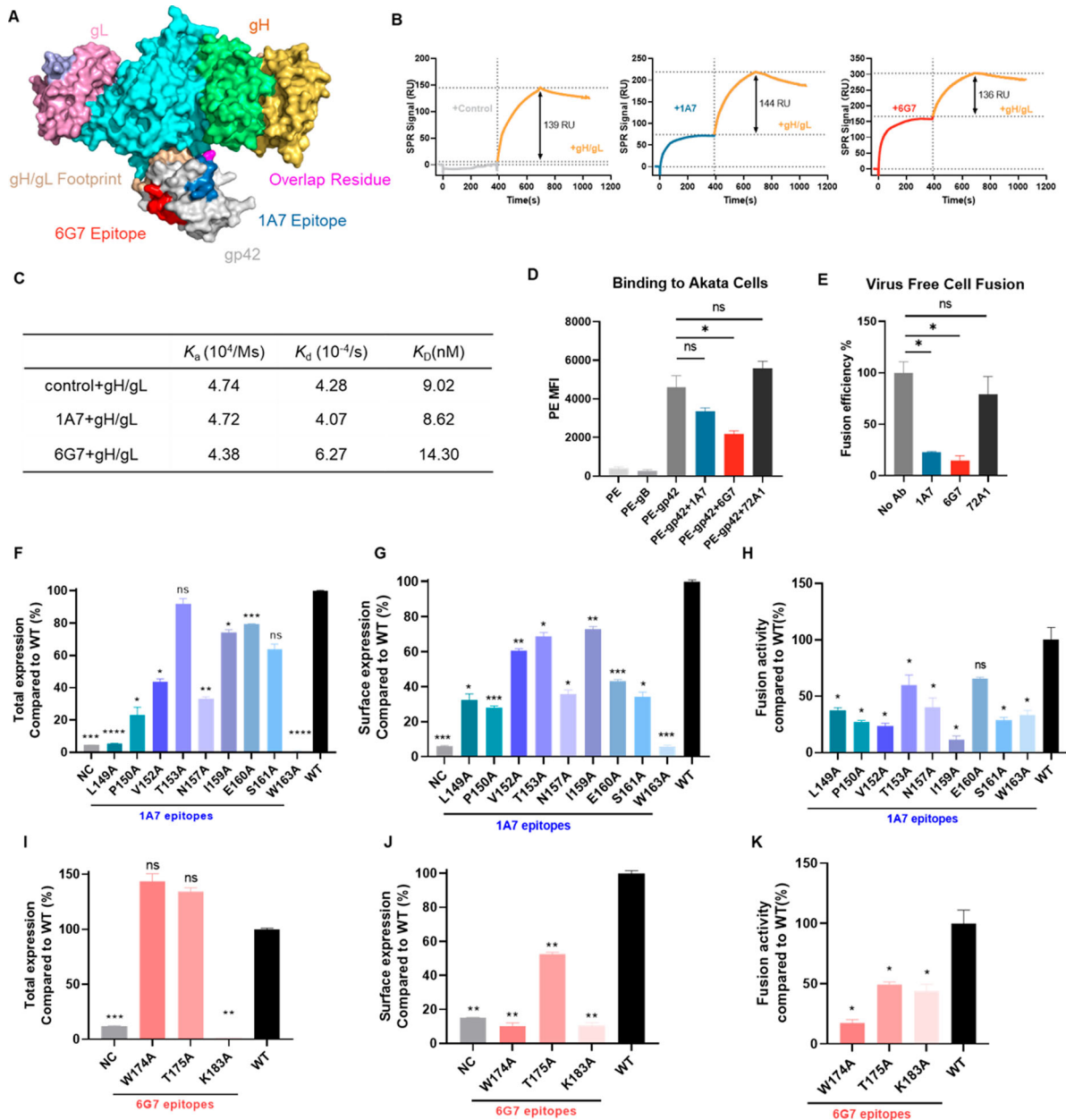
Figure 6. Different neutralizing mechanisms of 1A7 and 6G7. (A) Surface representation of gp42 and gH/gL proteins. gL is coloured in light pink and the four domains of gH are coloured in light blue, cyan, green and yellow in order. gp42 is coloured in grey with the gH/gL footprint shown in light orange. The 1A7 and 6G7 epitopes are coloured as sky blue and red respectively. The overlapping residue (I159) of the 1A7 epitope and gH/gL footprint is coloured in pink. (B) SPR competition assays. Immobilized gp42 was saturated with antibodies 1A7 (blue) or 6D7 (red), or mock treated (grey) for 400 s before the addition of soluble gH/gL. RU signals corresponding to the amount of gH/gL bound after 300 s are indicated. (C) Kinetic and affinity values of gp42 binding to gH/gL determined by SPR in the presence or absence of antibodies. (D) Akata cells were stained with PE-conjugated gp42 with or without the indicated antibodies. Anti-gp350 neutralizing antibody 72A1 was used as a negative control for interference with PE-gp42 binding. PE-labelled gB is used as a negative control for staining. Mean fluorescence intensity of stained cells is shown. Bars represent the average of two experiments ± SEM. (E) Inhibition of membrane fusion of MAbs was evaluated in a virus-free cell fusion assay. Transfected 293T cells are used to recapitulate HLA-II-dependent membrane fusion that occurs during EBV infection of B cells. Fusion of effector cells expressing EBV gB, gH, gL and gp42 with target cells expressing HLA-II is recorded using a luciferase-based assay (see Material and Methods). Fusion is reported as percentage of fusion in the absence of antibody. Anti-gp350 neutralizing antibody 72A1 was used as a negative control. Total expression and surface expression levels of gp42 mutated in epitopes recognized by 1A7 (F and G) and 6G7 (I and J) were analysed by flow cytometry. All values were normalized as percentages of wild type gp42 (WT). (H and K) Cell-cell fusion efficiencies of wild type gp42 (WT) and gp42 mutants were evaluated in a virus-free B cell fusion assay. All values were normalized as percentages of wild type gp42 (WT). P values from the unpaired Welch's t tests are indicated (significant difference is indicated by asterisks). ns, no significant difference. $*P \leq 0.0332$; $**P \leq 0.0021$; $***P \leq 0.0002$; $****P \leq 0.0001$. All data are presented as mean ± SEM.

(Figure 6(J,K)). The significant reduction of surface expression of W174A and T175A mutants indicated these residues may be essential for gp42 folding and membrane transportation. Collectively, 1A7 and 6G7 are capable of inhibiting membrane fusion and the key residues recognized by 1A7 and 6G7 are

important for gp42 expression, surface transportation and fusion activity.

The 1A7 and 6G7 epitopes constitute major targets for gp42-specific neutralization

In order to evaluate the immunodominance of epitopes recognized by 1A7 and 6G7, we conducted competition ELISA between gp42-immunized rabbit sera and the two monoclonal antibodies. The results showed that gp42-immunized rabbit sera significantly decreased the binding efficiency of 1A7 and 6G7, while control sera had no such effect (Figure 7(A,B)). These data suggest that anti-gp42 sera contained high amounts of 1A7- and 6G7-like antibodies recognizing similar epitopes. The regions recognized by 1A7 and 6G7 induced antibodies in total sera IgGs from immunized rabbits. To determine whether the antibodies induced by 1A7 and 6G7 epitopes had similar neutralizing ability *in vivo*, rabbits ($n = 5$ per group) were immunized with equimolar amounts of gp42 and gp42&Fab complex. The addition of 1A7-Fab and 6G7-Fab are anticipated to mask the corresponding epitopes and inhibit the generation of 1A7 and 6G7-like antibodies after immunization [53]. Indeed, anti-gp42 sera titres induced by gp42&Fab complexes were ~2–3 fold lower than titre induced by gp42 alone (Figure 7(C)). The neutralizing antibody titres were further assessed using the B cell infection model. Here, gp42 induced potent neutralizing antibody response against EBV-GFP infection of B cell, since 100-fold diluted sera achieved 85% neutralization (Figure 7(D)). By contrast, sera collected from rabbits immunized with gp42&1A7-Fab complex could only induce 35% neutralization (Figure 7(D)). Furthermore, gp42&6G7-Fab only barely induced neutralizing antibodies, indicating the major role of this epitope for neutralization, in accordance with neutralization by the cognate 6G7 antibody (Figure 1(G)). In agreement with these data, gp42&1A7&6G7-Fab also failed to induce a neutralizing antibody response (Figure 7(D)). These results demonstrated that the blockade by 1A7 and, in particular 6G7 significantly reduced the production of anti-gp42 NAbs. Taken together, the epitopes recognized by 1A7 and especially 6G7 are primary targets for the generation of EBV neutralizing antibodies.

To evaluate the immunodominance of the 1A7 and 6G7 epitopes during natural infections, we used a competitive binding assay between these antibodies and human sera from 16 EBV-positive healthy donors and 16 NPC patients (Figure 7(E)). When used as a competitor, 1A7 reduced the binding of gp42 to the serum antibodies of NPC patients (27.17% ± 4.02%) and healthy donors (28.37% ± 3.75%). A more effective competition was observed for 6G7 against serum antibodies from NPC patients (42.39% ± 5.05%) and

healthy donors (32.96% ± 8.31%). These results indicated that the epitopes on gp42 recognized by 1A7 and 6G7 are immunodominant in humans and induce antibody responses in health individuals and NPC patients.

In summary, these data demonstrated the immunodominance of the 6G7 and 1A7 epitopes in the production of neutralizing antibodies.

Discussion

Here, we isolated two EBV gp42-specific rabbit NAbs, 1A7 and 6G7, with nanomolar affinity for gp42, and defined new neutralizing epitopes on gp42 CTLD. Nab 6G7 effectively protected humanized mice from EBV viremia and EBV-induced lymphoma by inhibiting viral infection. Both 6G7 and 1A7 recognize different regions of gp42 in a glycosylation-independent manner. The interaction between 6G7 or 1A7 and gp42 did not affect the gH/gL-gp42 interaction. Key residues recognized by 6G7 and 1A7 were essential for gp42 expression, membrane transport and membrane fusion ability. Importantly, the epitopes recognized by 6G7 and 1A7 were predominant neutralizing epitopes recognized by antibodies from sera of gp42-immunized rabbits. These results will further guide the development of antiviral vaccine and therapeutics.

EBV is a ubiquitous oncogenic virus that causes great human diseases burden. It is usually acquired asymptomatically in children and establishes latent infection in B lymphocytes. Prophylactic vaccine against B cell infection is an ideal approach to prevent EBV latent infection and control reactivation [54]. The majority of previous EBV vaccine studies focused on gp350, which is the first identified and most abundant envelope glycoprotein [8,36]. However, the gp350-based vaccine failed to prevent asymptomatic EBV infection, which may still be a risk factor for inducing EBV-associated diseases [13]. Considering the abundance of gp350 on the viral envelope, gp350 may act as a decoy for antiviral humoral immunity. Similar to gp350, gp42 serves as a receptor binding glycoprotein [26]. Antibodies targeting gp42 in human sera contribute to virus-neutralizing activities [16], suggesting that gp42 is another important target of neutralizing antibodies. Nevertheless, gp42-specific antibodies have proven difficult to isolate from human PBMCs. So far, the reported anti-gp350 and anti-gp42 antibodies are all murine origin [55–57]. Nevertheless, rabbit antibodies have become increasingly popular and promising tools in laboratory research and clinical application due to their higher specificity, stronger affinity and greater diversity [58].

gp42 acts as the cell tropism switch for EBV infection, which is unique within the herpesvirus family. However, few NAbs targeting gp42 have been
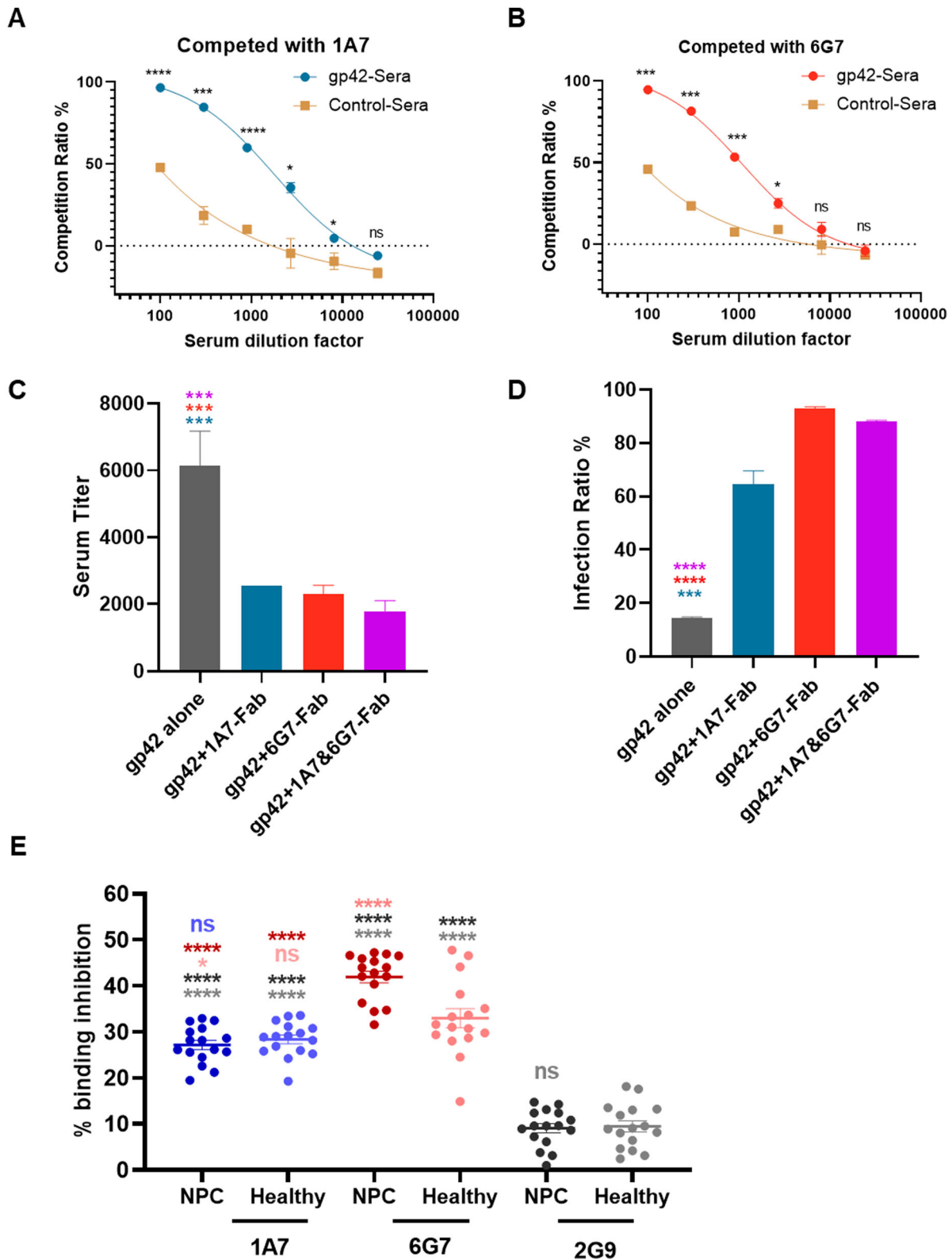
Figure 7. 1A7 and 6G7 epitopes are predominant neutralizing epitopes. (A and B) Epitope competition between gp42-immunized rabbit sera ($n = 3$) and 1A7 (A) or 6G7 (B) was evaluated by ELISA. Diluted gp42-immunized rabbit sera were co-incubated with constant amounts of HRP conjugated 1A7 or 6G7. The OD values of 1A7-HRP and 6G7-HRP were measured by ELISA in the presence or absence of sera. The data are presented as percent inhibition for each antibody. Preimmune sera were used as negative control. (C) Serum titres of gp42-specific antibodies in rabbit sera after immunization with gp42 or gp42-Fab complexes. Rabbits were immunized with equimolar amounts of gp42 and gp42&Fab complex ($n = 5$). (D) The neutralizing activities of sera were evaluated using B cell infection assay. Sera from 2 rabbits per group were used at 100-fold dilution. (E) Blocking naturally acquired anti-gp42 antibodies in human sera by 1A7 and 6G7 was evaluated by competitive ELISA. The anti-gp42 mAbs, 1A7 and 6G7, and an anti-influenza HA antibody 2G9 (negative control) were used to block the binding of recombinant gp42 to human serum antibodies. The binding of each serum to gp42 was measured by ELISA in the presence or absence of pre-incubation of gp42 with 1A7, 6G7 or 2G9. Data are shown as mean ± SEM. Statistical analyses were performed using one-way ANOVA. All data are presented as mean ± SEM. ns, no significant difference; *$P \le 0.0332$; ***$P \le 0.0002$; ****$P \le 0.0001$.

reported. In addition, no anti-gp42 antibody has been evaluated for protection *in vivo*. In this study, NAbs 1A7 and 6G7 potently neutralized B cells infection *in vitro* (Figure 1(F)). The chimeric 6G7 showed potent protection against lethal EBV challenge and efficiently prevented the formation of lymphomas in mouse spleens through inhibiting viral infection (Figure 2 and 3). Furthermore, in humanized mice, 6G7 showed a comparable protection potency to AMMO1, an anti-gH/gL NAb that protects against virus challenge in both humanized mouse and rhesus macaque infection models [45]. Indeed, immunogens combining gH/gL and gp42 induced high B-cell-neutralizing titres [16], suggesting synergistic activities of anti-gH/gL and anti-gp42 antibodies. The antibody cocktail containing the two potent NAbs 6G7 and AMMO1 would provide a promising therapeutic combination since they are capable of neutralizing EBV infection via different mechanisms.

The C-terminal domain of gp42 plays a crucial role in receptor binding and therefore is considered the major target for anti-gp42 NAbs [23,26,33,57]. The N-terminal domain of gp42 is essential for tethering gH/gL [56]. However, we previously generated a panel of antibodies targeting the N-terminal domain and none of them showed neutralizing ability [56]. F-2-1 was the first reported anti-gp42 NAb, and its epitope within the C-terminal domain of gp42 while the accurate epitope of F-2-1 remains unknown [23,57]. In this study, 1A7 and 6G7 defined two distinct neutralizing epitopes in the C-terminal domain of gp42 (Figure 4 and Fig. S6). The precise epitopes of 1A7 and 6G7 have been localized at [149]LPVVTRNLNAIESLW[163] and [174]WTSLDGGTFK[183], respectively. Interestingly, these antibodies did not cross-react with rhLCV gp42 even though the corresponding regions on rhLCV gp42 share high sequence identity ([148]LPVVTGNLKA-SESLW[162] and [173]WTSLDGGNYQ[182]) (Fig. S2). Accordingly, key residues N157 and I159 in the 1A7 epitope, and K183 in the 6G7 epitope differ in rhLCV gp42 (K156, S158 and Q182, respectively) (Fig. S2). This comparison suggests that these key residues contribute to the specificity of 1A7 and 6G7 for EBV gp42.

The glycosylation of glycoproteins plays critical roles in virulence and immune evasion for many viruses including EBV [52]. gp350 is a heavily glycosylated protein and its glycosylation is essential for maintaining its antigenicity and immunogenicity [38]. Unglycosylated gp350 produced from *E. coli* did not react with NAb 72A1, suggesting that glycosylation contributes to maintaining conformation-specific epitopes [59]. During EBV entry, gL is involved in gB-mediated membrane fusion by direct interaction with gB. Interestingly, the gL deglycosylation mutant N69L/S71V showed a hyperfusogenic phenotype [29,60], indicating that gL glycosylation is one of the key regulators of EBV membrane fusion.

gp42 directly blocks the interaction of HLA-II & peptides complexes with TCR to contribute to immune evasion [23,25]. gp42 contains four glycosylation sites, which functions are unclear [26]. Here, we investigated the impact of deglycosylation on gp42 function. Surprisingly, the deglycosylation treatment did not impair the antigenicity of gp42 and its ability to bind gH/gL (Figure 5(C,D)), indicating that the gp42 glycosylation was not necessary for the formation of the gH/gL-gp42 complex. Despite the glycosylation sites locating near the 1A7 and 6G7 epitopes, the removal of carbogydrates from gp42 had no effect on 1A7 and 6G7 binding (Figure 5(E)), suggesting that N-glycosylation of gp42 also did not participate in the recognition by these antibodies.

The gH/gL/gp42 entry complex is required for B cell infection [18]. The binding affinity between gH/gL and gp42 was not altered by pre-incubation with 1A7 or 6G7 (Figure 6(C)), suggesting that the antibodies did not affect the gH/gL-gp42 interaction. However, pre-incubation of 6G7 inhibited gp42 binding to the B cell surface while 1A7 did not, even though the 1A7 epitope partially overlap with the HLA-II binding site (Fig. S7A). The molecule docking result provided a possible antibody-binding model of 1A7 and 6G7, and there may be a potential clash between HLA-II and 1A7 (Fig. S7B). Similarly, the epitope of the anti-gH/gL NAb AMMO1 overlaps with the gp42 binding site but did not affect the formation of gH/gL/gp42 complex [27], indicating that overlapping epitopes do not always directly block interactions. The key residues recognized by 1A7 and 6G7 are important for gp42 expression, surface transportation and fusion activity. Despite its inability to prevent gp42 binding to B cells, 1A7 efficiently inhibited membrane fusion with B cells, similarly to 6G7 (Figure 6(E)). The different inhibitory activities of 1A7 against cell surface binding and membrane fusion may suggest that 1A7 could disturb membrane fusion without blocking HLA-II binding (Figure 6). 1A7 could possibly restrict signal transmission from the gH/gL/gp42 complex to gB and prevent gB activation. Considering that the epitope recognized by 6G7 was distant from HLA-II binding site, 6G7 could also prevent gB activation by gH/gL/gp42, or restrict access of gp42 to HLA-II by creating steric hindrance through its Fc fragment. However, detailed structural analysis determined by cryo-electron microscopy or X-ray is needed to identify the accurate binding sites, and to illustrate the accurate neutralizing mechanisms of the new 1A7 and 6G7 antibodies.

The epitopes recognized by 1A7 and 6G7 are accessible and immunogenic following immunization with native gp42. Both 1A7 and 6G7 could recognize gp42 displayed on cell surfaces, indicating their epitopes were accessible in native form (Figure 1(C,D)).

Competition experiments between gp42-immunized sera and anti-gp42 NAbs showed that antibodies sharing epitopes with 1A7 and 6G7 represented a major proportion of total anti-gp42 antibodies (Figure 7(A, B)). In addition, we identified the essential role of C-terminal domain of gp42, especially the epitopes recognized by 1A7 and 6G7, in generating NAbs against EBV infection (Figure 7). The epitope recognized by 6G7 may induce more potent NAbs than the 1A7 epitope, which is consistent with their relative neutralizing potency (Figure 1(F) and Figure 7). Together, 1A7 and 6G7 defined two predominant neutralizing epitopes on gp42. Strategies to design immunogens targeting the gp42 epitopes recognized by 1A7 and 6G7 may provide promising options for prophylactic EBV vaccines.

In summary, we reported two anti-gp42 NAbs, 1A7 and 6G7, which show neutralization against EBV infection of B cells. 6G7 exhibits potent protection efficiency against a lethal EBV challenge in humanized mice by inhibiting viral infection and preventing tumour formation. Mapping 1A7 and 6G7 epitopes uncovered two novel and predominant neutralizing epitopes, and each antibody may exert neutralization using a different mechanism. This study provides new insight into rational design for vaccines and therapeutics against EBV infection.

ORCID

Ningshao Xia http://orcid.org/0000-0003-0179-5266

References

[1] Cohen JI, Fauci AS, Varmus H, et al. Epstein-Barr virus: an important vaccine target for cancer prevention. Sci Transl Med. 2011 Nov 2;3(107):107fs7. doi:10.1126/scitranslmed.3002878

[2] Dunmire SK, Verghese PS, Balfour HH, Jr. Primary Epstein-Barr virus infection. J Clin Virol. 2018 May;102:84–92. doi:10.1016/j.jcv.2018.03.001

[3] Schmitz H, Volz D, Krainick-Riechert C, et al. Acute Epstein-Barr virus infections in children. Med Microbiol Immunol. 1972;158(1):58–63. doi:10.1007/BF02122009

[4] Khan G, Fitzmaurice C, Naghavi M, et al. Global and regional incidence, mortality and disability-adjusted life-years for Epstein-Barr virus-attributable malignancies, 1990–2017. BMJ Open. 2020 Aug 30;10(8):e037505. doi:10.1136/bmjopen-2020-037505

[5] Bjornevik K, Cortese M, Healy BC, et al. Longitudinal analysis reveals high prevalence of Epstein-Barr virus associated with multiple sclerosis. Science. 2022 Jan 21;375(6578):296–301. doi:10.1126/science.abj8222

[6] Zhong L, Zhao Q, Zhang X. Unmasking the enigma: Epstein-Barr virus as a primary trigger in multiple sclerosis. J Autoimmune Disord. 2023 Jun 14;9(2):31.

[7] Gold JE, Okyay RA, Licht WE, et al. Investigation of long COVID prevalence and its relationship to Epstein-Barr virus reactivation. Pathogens. 2021 Jun 17;10(6):763. doi:10.3390/pathogens10060763

[8] Zhong L, Krummenacher C, Zhang W, et al. Urgency and necessity of Epstein-Barr virus prophylactic vaccines. NPJ Vaccines. 2022 Dec 9;7(1):159. doi:10.1038/s41541-022-00587-6

[9] Zhong L, Zhang W, Krummenacher C, et al. Targeting herpesvirus entry complex and fusogen glycoproteins with prophylactic and therapeutic agents. Trends Microbiol. 2023 Mar 24;31(8):788–804. doi:10.1016/j.tim.2023.03.001

[10] Tarbouriech N, Buisson M, Géoui T, et al. Structural genomics of the Epstein-Barr virus. Acta Crystallogr D Biol Crystallogr. 2006 Oct;62(Pt 10):1276–1285. doi:10.1107/S0907444906030034

[11] Johannsen E, Luftig M, Chase MR, et al. Proteins of purified Epstein-Barr virus. Proc Natl Acad Sci U S A. 2004 Nov 16;101(46):16286–16291. doi:10.1073/pnas.0407320101

[12] Tanner J, Weis J, Fearon D, et al. Epstein-Barr virus gp350/220 binding to the B lymphocyte C3d receptor mediates adsorption, capping, and endocytosis. Cell. 1987 Jul 17;50(2):203–213. doi:10.1016/0092-8674(87)90216-9

[13] Moutschen M, Léonard P, Sokal EM, et al. Phase I/II studies to evaluate safety and immunogenicity of a recombinant gp350 Epstein-Barr virus vaccine in healthy adults. Vaccine. 2007 Jun 11;25(24):4697–4705. doi:10.1016/j.vaccine.2007.04.008

[14] Janz A, Oezel M, Kurzeder C, et al. Infectious Epstein-Barr virus lacking major glycoprotein BLLF1 (gp350/220) demonstrates the existence of additional viral ligands. J Virol. 2000 Nov;74(21):10142–10152. doi:10.1128/JVI.74.21.10142-10152.2000

[15] Wang X, Hutt-Fletcher LM. Epstein-Barr virus lacking glycoprotein gp42 can bind to B cells but is not able to infect. J Virol. 1998 Jan;72(1):158–163. doi:10.1128/JVI.72.1.158-163.1998

[16] Bu W, Joyce MG, Nguyen H, et al. Immunization with components of the viral fusion apparatus elicits

antibodies that neutralize Epstein-Barr virus in B cells and epithelial cells. Immunity. 2019 May 21;50 (5):1305–1316.e6. doi:10.1016/j.immuni.2019.03.010

[17] Mohl BS, Chen J, Sathiyamoorthy K, et al. Structural and mechanistic insights into the tropism of Epstein-Barr virus. Mol Cells. 2016 Apr 30;39(4):286–291. doi:10.14348/molcells.2016.0066

[18] Sathiyamoorthy K, Jiang J, Hu YX, et al. Assembly and architecture of the EBV B cell entry triggering complex. PLoS Pathog. 2014 Aug;10(8):e1004309. doi:10.1371/journal.ppat.1004309

[19] Machiels B, Stevenson PG, Vanderplasschen A, et al. A gammaherpesvirus uses alternative splicing to regulate its tropism and its sensitivity to neutralization. PLoS Pathog. 2013 Oct;9(10):e1003753. doi:10.1371/journal.ppat.1003753

[20] Borza CM, Hutt-Fletcher LM. Alternate replication in B cells and epithelial cells switches tropism of Epstein-Barr virus. Nat Med. 2002 Jun;8(6):594–599. doi:10.1038/nm0602-594

[21] Rowe CL, Matsuura H, Jardetzky TS, et al. Investigation of the function of the putative self-association site of Epstein-Barr virus (EBV) glyco-protein 42 (gp42). Virology. 2011 Jul 5;415(2):122–131. doi:10.1016/j.virol.2011.04.003

[22] Sorem J, Jardetzky TS, Longnecker R. Cleavage and secretion of Epstein-Barr virus glycoprotein 42 promote membrane fusion with B lymphocytes. J Virol. 2009 Jul;83(13):6664–6672. doi:10.1128/JVI.00195-09

[23] Ressing ME, van Leeuwen D, Verreck FA, et al. Epstein-Barr virus gp42 is posttranslationally modified to produce soluble gp42 that mediates HLA class II immune evasion. J Virol. 2005 Jan;79 (2):841–852. doi:10.1128/JVI.79.2.841-852.2005

[24] Ressing ME, van Gent M, Gram AM, et al. Immune evasion by Epstein-Barr virus. Curr Top Microbiol Immunol. 2015;391:355–381.

[25] Ressing ME, van Leeuwen D, Verreck FA, et al. Interference with T cell receptor-HLA-DR interactions by Epstein-Barr virus gp42 results in reduced T helper cell recognition. Proc Natl Acad Sci USA. 2003 Sep 30;100(20):11583–11588. doi:10.1073/pnas.2034960100

[26] Mullen MM, Haan KM, Longnecker R, et al. Structure of the Epstein-Barr virus gp42 protein bound to the MHC class II receptor HLA-DR1. Mol Cell. 2002 Feb;9(2):375–385. doi:10.1016/S1097-2765(02)00465-3

[27] Snijder J, Ortego MS, Weidle C, et al. An antibody targeting the fusion machinery neutralizes dual-tropic infection and defines a site of vulnerability on Epstein-Barr virus. Immunity. 2018 Apr 17;48 (4):799–811.e9. doi:10.1016/j.immuni.2018.03.026

[28] Shaw PL, Kirschner AN, Jardetzky TS, et al. Characteristics of Epstein-Barr virus envelope protein gp42. Virus Genes. 2010 Jun;40(3):307–319. doi:10.1007/s11262-010-0455-x

[29] Sathiyamoorthy K, Hu YX, Möhl BS, et al. Structural basis for Epstein-Barr virus host cell tropism mediated by gp42 and gHgL entry glycoproteins. Nat Commun. 2016 Dec 8;7:13557. doi:10.1038/ncomms13557

[30] Rowe CL, Chen J, Jardetzky TS, et al. Membrane anchoring of Epstein-Barr virus gp42 inhibits fusion with B cells even with increased flexibility allowed by engineered spacers. mBio. 2015 Jan 6;6(1). doi:10.1128/mbio.02285-14

[31] Kirschner AN, Lowrey AS, Longnecker R, et al. Binding-site interactions between Epstein-Barr virus fusion proteins gp42 and gH/gL reveal a peptide that inhibits both epithelial and B-cell membrane fusion. J Virol. 2007 Sep;81(17):9216–9229. doi:10.1128/JVI.00575-07

[32] Liu F, Marquardt G, Kirschner AN, et al. Mapping the N-terminal residues of Epstein-Barr virus gp42 that bind gH/gL by using fluorescence polarization and cell-based fusion assays. J Virol. 2010 Oct;84 (19):10375–10385. doi:10.1128/JVI.00381-10

[33] Kirschner AN, Sorem J, Longnecker R, et al. Structure of Epstein-Barr virus glycoprotein 42 suggests a mechanism for triggering receptor-activated virus entry. Structure. 2009 Feb 13;17(2):223–233. doi:10.1016/j.str.2008.12.010

[34] McShane MP, Mullen MM, Haan KM, et al. Mutational analysis of the HLA class II interaction with Epstein-Barr virus glycoprotein 42. J Virol. 2003 Jul;77(13):7655–7662. doi:10.1128/JVI.77.13.7655-7662.2003

[35] Spriggs MK, Armitage RJ, Comeau MR, et al. The extracellular domain of the Epstein-Barr virus BZLF2 protein binds the HLA-DR beta chain and inhibits antigen presentation. J Virol. 1996 Aug;70 (8):5557–5563. doi:10.1128/jvi.70.8.5557-5563.1996

[36] Silva AL, Omerovic J, Jardetzky TS, et al. Mutational analyses of Epstein-Barr virus glycoprotein 42 reveal functional domains not involved in receptor binding but required for membrane fusion. J Virol. 2004 Jun;78(11):5946–5956. doi:10.1128/JVI.78.11.5946-5956.2004

[37] Lanzavecchia A, Fruhwirth A, Perez L, et al. Antibody-guided vaccine design: identification of protective epitopes. Curr Opin Immunol. 2016 Aug;41:62–67. doi:10.1016/j.coi.2016.06.001

[38] Szakonyi G, Klein MG, Hannan JP, et al. Structure of the Epstein-Barr virus major envelope glycoprotein. Nature Struct Mol Biol. 2006 Nov;13(11):996–1001. doi:10.1038/nsmb1161

[39] Hong J, Wang Q, Wu Q, et al. Rabbit monoclonal antibody specifically recognizing a linear epitope in the RBD of SARS-CoV-2 spike protein. Vaccines. 2021 Jul 28;9(8):829. doi:10.3390/vaccines9080829

[40] Hoffman GJ, Lazarowitz SG, Hayward SD. Monoclonal antibody against a 250,000-dalton glyco-protein of Epstein-Barr virus identifies a membrane antigen and a neutralizing antigen. Proc Natl Acad Sci USA. 1980 May;77(5):2979–2983. doi:10.1073/pnas.77.5.2979

[41] Strnad BC, Schuster T, Klein R, et al. Production and characterization of monoclonal antibodies against the Epstein-Barr virus membrane antigen. J Virol. 1982 Jan;41(1):258–264. doi:10.1128/jvi.41.1.258-264.1982

[42] Kirschner AN, Omerovic J, Popov B, et al. Soluble Epstein-Barr virus glycoproteins gH, gL, and gp42 form a 1:1:1 stable complex that acts like soluble gp42 in B-cell fusion but not in epithelial cell fusion. J Virol. 2006 Oct;80(19):9444–9454. doi:10.1128/JVI.00572-06

[43] Guo S, Gao S, Liu R, et al. Oncological and genetic factors impacting PDX model construction with NSG mice in pancreatic cancer. FASEB J. 2019 Jan;33 (1):873–884. doi:10.1096/fj.201800617R

[44] Hong J, Zhong L, Zheng Q, et al. A neutralizing antibody targeting gH provides potent protection against

EBV challenge in vivo. J Virol. 2022 Apr 27;96(8): e0007522. doi:10.1128/jvi.00075-22

[45] Singh S, Homad LJ, Akins NR, et al. Neutralizing antibodies protect against oral transmission of lymphocryptovirus. Cell Rep Med. 2020 Jun 23;1(3). doi:10.1016/j.xcrm.2020.100033

[46] Mgodi NM, Takuva S, Edupuganti S, et al. A phase 2b study to evaluate the safety and efficacy of VRC01 broadly neutralizing monoclonal antibody in reducing acquisition of HIV-1 infection in women in sub-Saharan Africa: baseline findings. J Acquir Immune Defic Syndr. 2021 May 1;87(1):680–687. doi:10.1097/QAI.0000000000002649

[47] Chen H, Zhong L, Zhang W, et al. Dose-dependent outcome of EBV infection of humanized mice based on green Raji unit (GRU) doses. Viruses. 2021 Oct 29;13(11):2184.

[48] Chatterjee B, Leung CS, Munz C. Animal models of Epstein Barr virus infection. J Immunol Methods. 2014 Aug;410:80–87. doi:10.1016/j.jim.2014.04.009

[49] Munz C. EBV infection of mice with reconstituted human immune system components. Curr Top Microbiol Immunol. 2015;391:407–423.

[50] De Paschale M, Clerici P. Serological diagnosis of Epstein-Barr virus infection: problems and solutions. World J Virol. 2012 Feb 12;1(1):31–43. doi:10.5501/wjv.v1.i1.31

[51] Rivailler P, Jiang H, Cho YG, et al. Complete nucleotide sequence of the rhesus lymphocryptovirus: genetic validation for an Epstein-Barr virus animal model. J Virol. 2002 Jan;76(1):421–426. doi:10.1128/JVI.76.1.421-426.2002

[52] Watanabe Y, Bowden TA, Wilson IA, et al. Exploitation of glycosylation in enveloped virus pathobiology. Biochim Biophys Acta Gen Subj. 2019 Oct;1863 (10):1480–1497. doi:10.1016/j.bbagen.2019.05.012

[53] Xing Y, Oliver SL, Nguyen T, et al. A site of varicella-zoster virus vulnerability identified by structural studies of neutralizing antibodies bound to the glycoprotein complex gHgL. Proc Natl Acad Sci USA. 2015 May 12;112(19):6056–6061. doi:10.1073/pnas.1501176112

[54] Jean-Pierre V, Lupo J, Buisson M, et al. Main targets of interest for the development of a prophylactic or therapeutic Epstein-Barr virus vaccine. Front Microbiol. 2021;12:701611.

[55] Slabik C, Kalbarczyk M, Danisch S, et al. CAR-T cells targeting Epstein-Barr virus gp350 validated in a humanized mouse model of EBV infection and lymphoproliferative disease. Mol Ther Oncolytics. 2020 Sep 25;18:504–524. doi:10.1016/j.omto.2020.08.005

[56] Hong J, Wei D, Wu Q, et al. Antibody generation and immunogenicity analysis of EBV gp42 N-terminal region. Viruses. 2021 Nov 28;13(12):2380. doi:10.3390/v13122380

[57] Li Q, Spriggs MK, Kovats S, et al. Epstein-Barr virus uses HLA class II as a cofactor for infection of B lymphocytes. J Virol. 1997 Jun;71(6):4657–4662. doi:10.1128/jvi.71.6.4657-4662.1997

[58] Weber J, Peng H, Rader C. From rabbit antibody repertoires to rabbit monoclonal antibodies. Exp Mol Med. 2017 Mar 24;49(3):e305. doi:10.1038/emm.2017.23

[59] Servat E, Ro BW, Cayatte C, et al. Identification of the critical attribute(s) of EBV gp350 antigen required for elicitation of a neutralizing antibody response in vivo. Vaccine. 2015 Nov 27;33(48):6771–6777. doi:10.1016/j.vaccine.2015.10.024

[60] Möhl BS, Chen J, Park SJ, et al. Epstein-Barr virus fusion with epithelial cells triggered by gB is restricted by a gL glycosylation site. J Virol. 2017 Dec 1;91(23). doi:10.1128/jvi.01255-17